

SAP-CoPE: Social-Aware Planning using Cooperative Pose Estimation with Infrastructure Sensor Nodes

Minghao Ning^{1†}, Yufeng Yang^{1*†}, Shucheng Huang¹, Jiaming Zhong¹, Keqi Shu¹, Chen Sun², Ehsan Hashemi³, *Senior Member, IEEE*, and Amir Khajepour¹, *Senior Member, IEEE*

Abstract—Autonomous driving systems must operate smoothly in human-populated indoor environments, where challenges arise including limited perception and occlusions when relying only on onboard sensors, as well as the need for socially compliant motion planning that accounts for human psychological comfort zones. These factors complicate accurate recognition of human intentions and the generation of comfortable, socially aware trajectories. To address these challenges, we propose SAP-CoPE, an indoor navigation system that integrates cooperative infrastructure with a novel 3D human pose estimation method and a socially-aware model predictive control (MPC)–based motion planner. In the perception module, an optimization problem is formulated to account for uncertainty propagation in the camera projection matrix while enforcing human joint coherence. The proposed method is adaptable to both single- and multi-camera configurations and can incorporate sparse LiDAR point-cloud data. For motion planning, we integrate a psychology inspired personal-space field using the information from estimated human poses into an MPC framework to enhance socially comfort in human-populated environments. Extensive real-world evaluations demonstrate the effectiveness of the proposed approach in generating socially aware trajectories for autonomous systems.

Note to Practitioners—Indoor autonomous mobile robots operating in public facilities such as hospitals must navigate crowded environments where onboard sensing is often challenged by occlusions and limited fields of view, while also accounting for human comfort in addition to collision avoidance. This paper presents SAP-CoPE, a deployable framework that integrates cooperative infrastructure sensing with socially aware motion planning. Ceiling-mounted sensor nodes provide expanded and occlusion-robust perception through uncertainty-aware 3D human pose estimation from cameras, optionally supplemented by sparse LiDAR data. Leveraging these pose estimates, an MPC-based planner incorporating a human personal space field generates trajectories that balance social comfort, efficiency, and safety while respecting the robot’s kinematic constraints. The proposed architecture is modular and compatible with existing indoor robotic platforms using standard hardware, and real-world experiments demonstrate smoother navigation and improved clearance and travelling time performance compared with conventional baseline methods.

Index Terms—Cooperative Perception, Human Pose Estimation, Social-awareness, Motion Planning, Model Predictive Control (MPC).

I. INTRODUCTION

Intelligent indoor mobility systems are gaining increasing attention in healthcare, logistics, and the automotive industry [1]–[3]. These systems reduce manual transportation tasks, minimize workplace injuries and improve operational efficiency [4]. In restricted environments, mobile robots primarily focus on avoiding collisions with objects and are programmed to stop when humans are nearby. However, this strategy is less effective in public areas like hospitals and shopping malls, where interactions with people are unavoidable. To enable safe and efficient human-robot interaction, such a system requires real-time obstacle detection, accurate human intention prediction, and a robust motion planning algorithm for safe and smooth navigation.

Recent research has been enhancing the perception ability of a robot through high-end onboard sensors; however, these systems still have limitations in perception range and field of view (FOV), especially in crowded indoor spaces [5]. Ning et al. introduced the Infrastructure Sensor Nodes (ISNs) system, ceiling-mounted multi-modal sensors perform local processing of raw data before transmitting concise perception outputs to a central cloud [6]. This architecture effectively expands the FOV, mitigates occlusions, and offers a cost-efficient alternative to high-end onboard sensing systems. However, accurately estimating pedestrian’s position and heading in the world coordinate using cost-efficient sensors remains a significant challenge. This information is critical to understand human intentions, which in turn enables proactive navigation and effective collision avoidance [7]. To address this, we propose a 3D pose estimation approach using probabilistic fusion of image and sparse point cloud data, ensuring real-time, accurate human pose detection.

On the other hand, Yang et al. [8] previously introduced a Model Predictive Control (MPC)-based motion planning algorithm that treats all objects as obstacles, prioritizing only physical safety. However, research shows that people maintain social zones in shared spaces [9], highlighting that psychological safety is equally important when navigating interactions with humans. To address this, we integrate a personal space concept from psychology studies into motion planning,

[†] indicates equal contribution

^{*} indicates the corresponding author

¹Minghao Ning, Yufeng Yang, Shucheng Huang, Jiaming Zhong, Keqi Shu and Amir Khajepour are with the Mechanical and Mechatronics Eng. Department, University of Waterloo, 200 University Ave W, Waterloo, ON N2L3G1, Canada. e-mail:{minghao.ning, f248yang, s95huang, j52zhong, keqi.shu, a.khajepour}@uwaterloo.ca).

²C. Sun is with the Department of Data and Systems Engineering, University of Hong Kong, Pok Fu Lam, Hong Kong, China (e-mail:c87sun@hku.hk)

³Ehsan Hashemi is with the Mechanical Engineering Department, University of Alberta, Alberta, T6G1H9, Canada (e-mail:ehashemi@ualberta.ca)

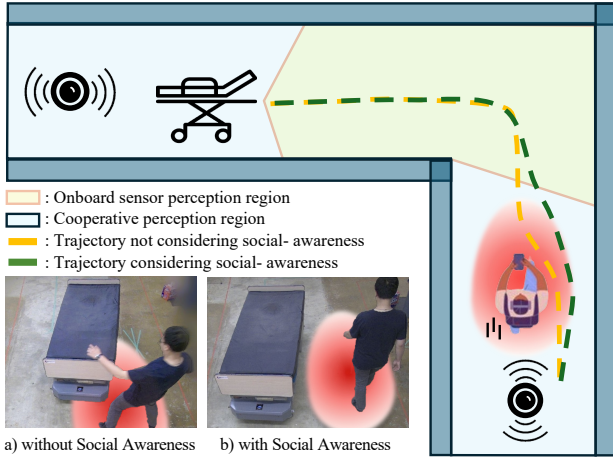


Fig. 1: Key challenges: (1) How to reliably detect humans in crowded, occluded scenarios? (2) How to guide the robot to human-comfortable motion?

enabling robots to respect social behaviour, and maintain comfortable distances in human-populated environments.

The key contributions of this article are as follows.

- 1) *Real-time Cooperative Perception System*: We proposed a cooperative perception framework that leverages sensor node networks to provide comprehensive environmental awareness.
- 2) *3D Human Pose Detection*: We develop a novel approach for 3D human pose detection that combines geometry-based techniques and sensor fusion between image data and sparse point clouds. This method enhances detection accuracy.
- 3) *Socially-aware Motion Planning Scheme*: We propose an MPC-based motion planning algorithm that integrates the personal space (PS) field to allow the robot to generate socially acceptable motion while accounting for the omnidirectional type robot's kinematic constraints to ensure the generation of feasible and practical motion of the robot. In addition, the considered PS model has an asymmetrical shape in the lateral direction, which can allow the smooth motion of the robot when encountering a large group of people.
- 4) *Validation through Real-world Experiments*: The proposed system is extensively validated through real-world experiments. Results demonstrate its accurate pose detection and effectiveness in handling human-robot interactions.

The structure of this article is organized as follows. Section II presents an overview of the proposed methodology. Section III details the perception algorithm. Section IV formulates the socially-aware motion planner. Section V presents the experimental results for the proposed system. Finally, Section VI concludes the study and discusses potential future research directions.

II. RELATED WORKS

A. Perception

Infrastructure-Based Perception Systems: Reliable perception is fundamental for intelligent indoor mobility systems.

Traditional infrastructure-based approaches, particularly those using vision sensors, have been widely explored. Works such as [10]–[13] employ ceiling or wall-mounted cameras to detect and track pedestrians. However, purely independent camera-driven systems can be sensitive to lighting conditions and occlusions, and they are generally limited to obtain precise 3D object positions without additional depth information. To overcome these limitations, researchers have explored multi-sensor fusion within the infrastructure. Brvsvic et al. [14] integrated RGB-D cameras, LiDAR, and marker-based tracking to enhance spatial accuracy and robustness. Though this approach improves performance, its scalability is hindered by high equipment and installation costs. Similarly, high-frequency motion capture systems [15] offer ground-truth level accuracy but are restricted to controlled spaces, limiting their practical use in real-world deployments. Overall, these limitations emphasize the demand for indoor perception systems that are both reliable under challenging conditions and feasible for cost-effective, large-scale deployment.

Cooperative Perception Systems: Cooperative perception improves environmental awareness by integrating sensory data from multiple sources, including other robots and infrastructure. This collaborative approach effectively addresses challenges such as occlusions and the limited FOV inherent in individual sensors. Recent advancements highlight the significance of Vehicle-to-Everything (V2X) in autonomous driving domain [16]–[19]. Huang et al. [17] highlight the critical role of data sharing between agents and infrastructure while identifying real-time performance and communication delay as key bottlenecks. Inspired by this concept, we propose a real-time cooperative perception system utilizing ceiling-mounted ISNs. Each node performs local perception and transmits lightweight observations to a central fusion module in real time. This architecture not only expands FOV and reduces occlusions in crowded indoor spaces, but also ensures timely and coherent perception by mitigating latency-induced errors in the fusion pipeline.

3D Human Pose Detection: Accurately estimating human 3D poses is vital for autonomous systems to interpret and predict human behavior, ensuring safe and socially aware interactions. Single camera-based methods have faced challenges such as depth ambiguity and occlusions [20], thus, the estimation accuracy can be enhanced by leveraging multi-modal sensor data. Zanfir et al. introduced HUM3DIL, a semi-supervised multi-modal approach that embeds LiDAR points into pixel-aligned multi-modal features and employs a Transformer architecture for prediction [21]. Similarly, Bauer et al. proposed a weakly supervised method that integrates camera and LiDAR data, enabling accurate 3D human pose estimation without extensive 3D annotations [22], however, it needs dense point cloud to generate high-accuracy pseudo 3D keypoint labels via projecting point cloud to image.

B. Planning

Social-aware Planning: Recent human-aware planning algorithms focus primarily on modeling human-robot interactions while often assuming the robot has a simple circular

shape for computational convenience, without explicitly accounting for rectangular or articulated platform geometries [23]–[26]. Among these algorithms, the Social Force Model (SFM) is widely used to generate socially acceptable robot motion. Kamezaki et al. [27] introduced a planning algorithm based on the inducible Social Force Model, while Ratsamne et al. [28] developed the Extended SFM (ESFM) by incorporating the human pose, orientation, etc. to improve the performance of conventional SFM. Despite their effectiveness, SFM-based approaches often model human influence as symmetric in all directions. While this assumption allows the robot to maintain distance from personal spaces in sparse environments, it can lead to frequent unexpected deceleration or even stopping in crowded settings, thereby reducing efficiency and increasing the risk of collisions.

Planning based on Information Types: Socially-aware planning algorithms can be broadly categorized into two types: individual state-based information and group-based information [29]. Individual state-based methods use detailed information such as position, pose, orientation, and velocity; for example, Stefanini et al. [30] proposed a novel planning algorithm that incorporates the articulated 3D human poses, semantic labels, and trajectory prediction to describe human behaviour. However, such approaches usually require reliable perception and tracking algorithms, and their performance can degrade significantly under occlusions, which are common in cluttered environments.

In contrast, group-based methods treat multiple humans as a single entity. Hoang et al. [31] opposed a proactive social motion model that accounts socio-spatiotemporal characteristics of human groups, allowing the mobile robot to plan a safe trajectory in various situations. Nevertheless, group-level representations may oversimplify complex interactions among individuals, potentially causing the robot to react conservatively or ignore subtle cues such as interpersonal distances, leader–follower structures, or individuals breaking away from the group.

On the other hand, although the above approaches have demonstrated strong performance in human-aware planning, they may not generalize well to large, rectangular robots with omnidirectional maneuverability, potentially resulting in unrealistic or impractical motions. Moreover, these methods often lack explicit constraints on robot kinematics and control limits, which may produce motion commands that are smooth in simulation but difficult to track reliably on actual hardware.

III. METHODOLOGY

The proposed SAP-CoPE method consists of two main systems: a real-time cooperative perception and a socially aware motion planning (Fig. 2). For the perception systems, it employs a group of multi-modal ISNs equipped with LiDAR, cameras, and edge computing for local object detection and 3D human pose estimation. A synchronized clock system aligns LiDAR scans with camera operations, ensuring temporally consistent data, which is transmitted to a Central Layer (CL) for global fusion, multi-object tracking, and delay compensation. For the motion-planning system, an MPC-based planner

is designed to generate optimal poses and is implemented in the CL, enabling the robot to compute a socially-aware motion that respects humans’ personal space while close to a predefined reference motion. To achieve this, the PS field inspired from psychology studies is incorporated into the MPC’s objective function.

Furthermore, the optimal control commands can then be obtained from the controller by tracking the motion generated from the planner. And these commands are then transmitted to the Application Layer (AL) for execution. In this study, the communication between the ISNs, CL, and AL is achieved using Wi-Fi network.

Additionally, the proposed SAP-CoPE framework is adaptable to various robotic platforms, such as the autonomous cart and autonomous medical bed at the Mechatronic Vehicle Systems Lab, University of Waterloo. In this study, only the autonomous medical bed [8] was used for experimental validation and is referred to as the term “robot” throughout this paper.

IV. PERCEPTION

A. Local Perception

The local perception consists of camera-based 2D detection, LiDAR point cloud processing, multi-modal class association, and a novel probabilistic 3D human pose estimation framework incorporating joint coherence constraints.

1) *Camera-based 2D Detection:* Recent advancements in deep learning have significantly improved camera-based 2D object detection. Notably, YOLOv11 [32] demonstrates superior accuracy and inference speed due to its state-of-the-art backbone and neck architectures. However, the pre-trained model does not generalize well to the top-down sensor node view and is unable to detect the autonomous robot used in our application. To address these limitations, we fine-tuned the YOLOv11 model using a dataset combining COCO [33] and the Indoor Cooperative Infrastructure Dataset (ICID) [6] to achieve human 2D pose detection and robot bounding box detection in one single network.

2) *LiDAR Processing and Class Association:* The LiDAR processing consists of region-of-interest filtering and a hierarchical clustering algorithm to group the points for obstacles while considering the scanning pattern. The clustering results are then fused with the camera-based 2D detection results for robot and human pose estimation. More details on the implementation of clustering and association can be found in our previous work [6]. The novel proposed 3D human pose estimation method is discussed in the following section.

3) *3D Human Pose Estimation with Joint Coherence Constraints:* Estimating absolute 3D human pose from a single camera is challenging due to the lack of depth information. As indicated in Fig. 2, our approach first obtains the 2D pixel coordinates of each joint and leverages prior height distribution information to estimate the rough 3D distribution of each joint as $P^i \sim N(\mu_{P^i}, \Sigma_{P^i})$ in the absolute world coordinate frame. This estimation is performed using the camera projection matrix H , ensuring a more robust and coherent 3D pose representation.

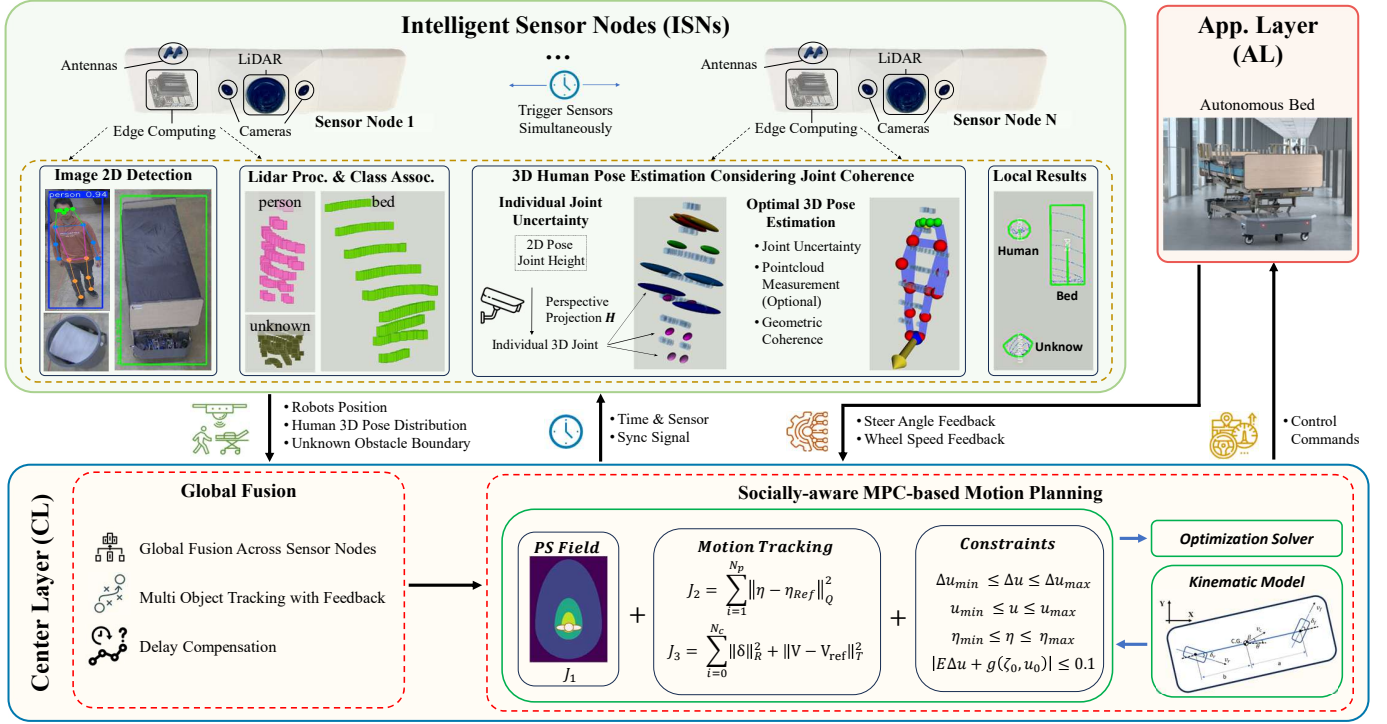


Fig. 2: SAP-CoPE Structure Overview

a) *World Coordinate and Jacobian Calculation:* Given a pixel point (x_p, y_p) , height information z_w , and the camera projection matrix H , we aim to estimate the world coordinates (x_w, y_w) and the Jacobian matrix \mathbf{J} of (x_w, y_w, z_w) with respect to (x_p, y_p, z_w) . The camera projection formula is given by:

$$s \begin{bmatrix} x_p \\ y_p \\ 1 \end{bmatrix} = K[R \ t] \begin{bmatrix} x_w \\ y_w \\ z_w \\ 1 \end{bmatrix} = H_{3 \times 4} \begin{bmatrix} x_w \\ y_w \\ z_w \\ 1 \end{bmatrix} \quad (1)$$

where s is a scale factor, x_p, y_p are the pixel coordinates, K is the camera intrinsic matrix, R is the rotation matrix, t is the translation vector, x_w, y_w, z_w are the world coordinates.

Given a projection matrix $H \in \mathbb{R}^{3 \times 4}$, which maps the 3D world coordinates to the 2D image plane, we denote its elements as follows:

$$H = \begin{bmatrix} h_{11} & h_{12} & h_{13} & h_{14} \\ h_{21} & h_{22} & h_{23} & h_{24} \\ h_{31} & h_{32} & h_{33} & h_{34} \end{bmatrix} \quad (2)$$

We define the intermediate variables:

$$\begin{aligned} a_{11} &= h_{31}x_p - h_{11}, & a_{12} &= h_{32}x_p - h_{12}, \\ a_{21} &= h_{31}y_p - h_{21}, & a_{22} &= h_{32}y_p - h_{22}, \\ b_1 &= h_{13}z_w - h_{33}x_p z_w - h_{34}x_p + h_{14}, \\ b_2 &= h_{23}z_w - h_{33}y_p z_w - h_{34}y_p + h_{24}. \end{aligned} \quad (3)$$

The world coordinates (x_w, y_w) are then calculated as:

$$\begin{aligned} x_w &= \frac{b_1 a_{22} - b_2 a_{12}}{a_{11} a_{22} - a_{12} a_{21}} = \frac{N_x}{D}, \\ y_w &= \frac{b_2 a_{11} - b_1 a_{21}}{a_{11} a_{22} - a_{12} a_{21}} = \frac{N_y}{D}. \end{aligned} \quad (4)$$

The Jacobian matrix \mathbf{J} of (x_w, y_w, z_w) with respect to (x_p, y_p, z_w) is given by:

$$\mathbf{J} = \begin{bmatrix} \frac{\partial x_w}{\partial x_p} & \frac{\partial x_w}{\partial y_p} & \frac{\partial x_w}{\partial z_w} \\ \frac{\partial y_w}{\partial x_p} & \frac{\partial y_w}{\partial y_p} & \frac{\partial y_w}{\partial z_w} \\ 0 & 0 & 1 \end{bmatrix} \quad (5)$$

This Jacobian matrix allows us to propagate uncertainties from the image plane to the world coordinates, essential for precise 3D pose estimation.

b) *Propagation of Uncertainty to 3D World Coordinates:* Building upon the computed world coordinates and the derived Jacobian matrix, we propagate the uncertainties of the input parameters (x_p, y_p, z_w) to estimate the 3D distribution of each joint in the absolute world coordinate system.

Using the Jacobian matrix \mathbf{J} , the covariance matrix of the estimated 3D position (x_w, y_w, z_w) is obtained through uncertainty propagation as: $\Sigma_{P^i} = \mathbf{J} \cdot \Sigma_{(x_p, y_p, z_w)} \cdot \mathbf{J}^T$, and the combined input uncertainty is defined as: $\Sigma_{(x_p, y_p, z_w)} = \text{diag}(\sigma_{x_p}^2, \sigma_{y_p}^2, \sigma_{z_w}^2)$.

The resulting covariance matrix Σ_{P^i} denotes the uncertainty in the world coordinates of the joint P^i . Combined with the mean position $\mu_{P^i} = [x_w, y_w, z_w]^T$, we represent the 3D position of each joint as a multivariate Gaussian distribution: $P^i \sim \mathcal{N}(\mu_{P^i}, \Sigma_{P^i})$.

c) *Joint Coherence in 3D Pose Estimation:* To maintain coherence in the inferred 3D human pose, we impose additional constraints based on the spatial relationships between adjacent joints. This is achieved by incorporating prior knowledge of bone lengths and their associated uncertainties. For example, given two adjacent joints P^i and P^j , the constraint on their Euclidean distance is modeled as: $\|\mu_{P^i} - \mu_{P^j}\| \approx l_{ij}$,

where l_{ij} is the prior mean of the bone length between the joints i and j . The uncertainty in l_{ij} is also incorporated, ensuring a consistent and biologically plausible pose.

d) *Final 3D Pose Estimation (Node Level)*: By combining the estimated 3D distributions $P^i \sim \mathcal{N}(\mu_{P^i}, \Sigma_{P^i})$ of individual joints with joint coherence constraints, we formulate a maximum likelihood estimation (MLE) problem to refine the entire 3D pose:

$$\begin{aligned} \arg \max_{\{\hat{\mu}_{P^i}\}} & \prod_i \exp\left(-\frac{1}{2}(\hat{\mu}_{P^i} - \mu_{P^i})^\top \Sigma_{P^i}^{-1}(\hat{\mu}_{P^i} - \mu_{P^i})\right) \\ & \cdot \prod_{i,j} \exp\left(-\frac{(\|\hat{\mu}_{P^i} - \hat{\mu}_{P^j}\| - l_{ij})^2}{2\sigma_{i,j}^2}\right) \\ & \cdot \prod_{k \in \mathcal{L}} \exp\left(-\frac{1}{2}(\hat{\mu}_{P^k} - \mu_{L^k})^\top \Sigma_{L^k}^{-1}(\hat{\mu}_{P^k} - \mu_{L^k})\right). \end{aligned} \quad (6)$$

where the last term represents an additional constraint imposed by LiDAR point cloud measurements. Here, \mathcal{L} denotes the subset of joints for which corresponding LiDAR measurements are available, μ_{L^k} represents the LiDAR-measured 3D joint positions, and Σ_{L^k} characterizes the measurement uncertainty associated with the LiDAR points.

This comprehensive approach enables robust estimation of absolute 3D human poses from single-camera setups by effectively integrating uncertainties, LiDAR measurements, and enforcing joint coherence constraints.

B. Delay-aware Global Perception

In ISNs system, computational and communication delays can introduce inconsistencies in perception, severely degrading the performance of following motion planning task. To address this, our previous work proposed a delay-aware cooperative perception pipeline that effectively mitigates latency effects and provides consistent, real-time perception outputs [6]. It contains three key components: global fusion across sensor nodes, multi-object tracking and delay compensation.

Each ISN sends its local perception results to the CL, and the detections are matched based on spatial proximity and class labels. For the objects detected by multiple ISNs, instead of simply averaging their positions like previous works [6], it refines the 3D human pose estimation via Eqn. 6 at the CL by fusing multi-view pose constraints from different ISNs to enhance robustness against occlusions and partial views.

Then, it performs multi-object tracking using an extended Kalman filter (EKF) for each detected object to keep track of their states over time. Human trajectories, in particular, are modeled using a non-linear dynamic system capable of capturing changes in walking direction and speed, which enhances robustness in crowded and dynamic environments.

To further improve real-time responsiveness, the system incorporates timestamp-based delay compensation. Each ISN assigns a local timestamp to detected objects, allowing the CL module to compute the delay relative to its current time. Object positions are then extrapolated forward using motion prediction models, effectively aligning stale data with the current system state. This compensation mechanism ensures

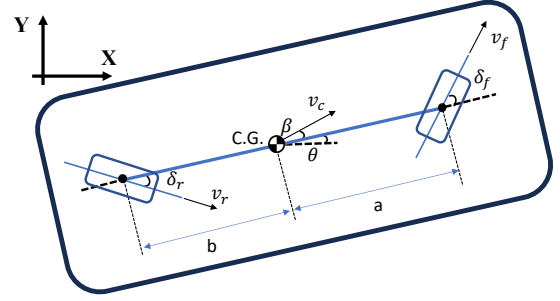


Fig. 3: Kinematic Motion Model of Robot

TABLE I: Personal Space Distance Specifications [34]

Types of Distance	Values	Relationship
Intimate distance	0 - 0.45 m	Very intimate relationship
Personal distance	0.45 - 1.2 m	Friends
Social distance	1.2 - 3.5 m	Strangers
Public distance	> 3.5 m	Public speaking

that the fused perception remains temporally consistent, even under variable network or processing latencies.

V. SOCIALLY-AWARE MOTION PLANNING

A. Kinematic-based Motion Model

In this paper, a kinematic model is used to describe the robot's motion as it operates at speeds below 5 km/h. The model is based on the assumptions of tire non-slippage and rigid body dynamics. Notably, the robot is capable of independently controlling the speed and steering angles of both the front and rear wheels, allowing it to have omnidirectional maneuverability. The kinematic model of the proposed robot is formulated as follows.

$$\beta = \tan^{-1}\left(\frac{l_r \tan(\delta_f) + l_f \tan(\delta_r)}{l_f + l_r}\right) \quad (7)$$

$$v_c = \frac{v_f \cos(\delta_f) + v_r \cos(\delta_r)}{2 \cos(\beta)} \quad (8)$$

$$\dot{X} = v_c \cos(\psi + \beta), \quad \dot{Y} = v_c \sin(\psi + \beta) \quad (9)$$

$$\dot{\psi} = \frac{v_f \sin(\delta_f) - v_r \sin(\delta_r)}{l_f + l_r} \quad (10)$$

Variables X and Y represent robot's position in the ground-fixed frame; ψ is the robot's yaw angle; β is the side-slip angle of C.G.; v_c is the C.G. velocity; l_f and l_r are the distances from the C.G. to the front and rear wheels; and v_f , v_r , δ_f , and δ_r are the velocity and steering of the front and rear wheels, respectively. In this paper, the system states, ξ , system outputs, η , and system control inputs, u_c are defined as follows.

$$\zeta = \eta = [X \quad Y \quad \psi]^T \quad (11)$$

$$u_c = [v_f \quad v_r \quad \delta_f \quad \delta_r]^T \quad (12)$$

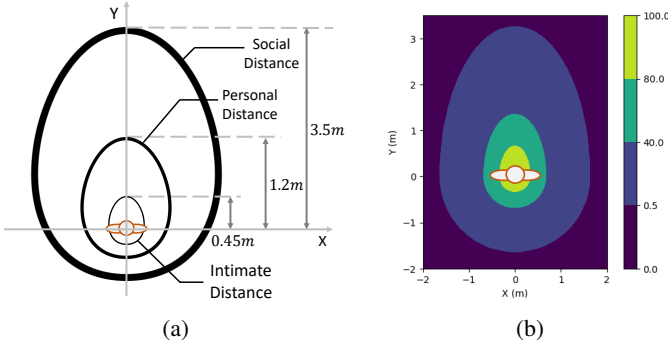


Fig. 4: Graphical Representation of Personal Space Field. a) Definition of Personal Field in psychology [34]. b) Constructed Personal Field using Mathematical Expression. In both figures, X and Y represent the body-fixed coordinate of the human.

B. Personal Space Field

This paper adapts the concept of personal space (PS) [34] to model human behaviour in interaction with the robot. Compare using the APF to represent the human, the PS model captures an individual's non-verbal and non-contact communication channels, influencing how they perceive proximity to others. Based on the studies from Edward T. Hall [35] and R. Sommer [36], PS can be divided into four regions: public distance, social distance, personal distance, and intimate distance. These regions define the various zones of comfort and social interaction. The graphical representation and the relative distances can be found in Fig. 4 a) and Table I.

By assigning appropriate values to each region, as shown in Fig. 4 b), the robot is able to maintain a psychologically safe distance from nearby humans. In this work, we adopt the asymmetric shaped field proposed in [34], where the field is intentionally shaped to be nonuniform in the y -direction and concentrated along the human's facing orientation. This design reflects the natural psychological comfort zones observed in human interactions, where individuals are more sensitive to being disturbed from the front. As a result, the robot can anticipate and steer earlier to avoid potential discomfort.

In contrast, the conventional SFM and Artificial Potential Field (APF) are normally symmetrical in both x and y directions, which requires enlarging the overall field size to achieve a similar early-dodging behavior from the robot. However, because the conventional field covers an equal area in front of and behind the human, it can lead to inefficient navigation behavior, such as unnecessary deceleration or even being trapped when operating in densely populated environments. The proposed PS field, therefore, enables more natural and efficient avoidance while ensuring safe interpersonal distances.

The formulation of the PS field can be found in the following. Let person P with pose $\{x_p, y_p\}$ at the position in the ground-fixed frame with heading angle θ_p ; and let another person Q at position of $\{x_q, y_q\}$ in the ground-fixed frame. The PS field of person P relative to person Q is denoted as Ω_{pq} , which is divided into two parts, where $\Omega_{pq,f}$ represents the front PS, and $\Omega_{pq,r}$ is the rear PS.

$$\Omega_{pq} = \gamma\Omega_{pq,f} + (1 - \gamma)\Omega_{pq,r} \quad (13)$$

Where, γ is a function of x_p , such that $\gamma(x_p) = 1$ if $d \geq 0$ and $\gamma(x_p) = 0$ otherwise. This relationship can be approximated by using the \tanh function in Equ. 14, where d is the relative position of person Q to person P in the body coordinate of person P , which can be expressed in Equ. 15. The variable k is a constant that controls the slope of the \tanh 's curve. To allow the γ becomes to 1 immediately when d is 0, we assigned a large value to k .

$$\gamma(x_p) = 0.5(\tanh(k \cdot d/2) + 1) \quad (14)$$

$$d = \begin{bmatrix} \cos \theta_p & \sin \theta_p \\ -\sin \theta_p & \cos \theta_p \end{bmatrix} \begin{bmatrix} x_q - x_p \\ y_q - y_p \end{bmatrix}. \quad (15)$$

On the other hand, each front and rear personal space $\Omega_{pq,i}, i \in \{f, r\}$ is defined as a 2D Gaussian function using the covariance matrix Σ and relative distance d .

$$\Omega_{pq,i} = e^{-0.5d^T \Sigma_i^{-1} d}, i \in \{f, r\} \quad (16)$$

Where, Σ_i defines the shape of the $\Omega_{pq,i}$. Based on the studies of Shozo [37], it is suggested that the front PS, $\Omega_{pq,f}$, of a human should be twice as large as the rear, left, and right sides. To implement this, the Σ_f and Σ_r are defined as follows, where $\sigma_{xx} = 2\sigma_{yy}$.

$$\Sigma_f = \begin{bmatrix} \sigma_{xx} & 0 \\ 0 & \sigma_{yy} \end{bmatrix}, \quad \Sigma_r = \begin{bmatrix} \sigma_{yy} & 0 \\ 0 & \sigma_{yy} \end{bmatrix} \quad (17)$$

Amaoka et al. [34] stated that the values of σ_{xx} should depend on several factors such as age, gender, etc.; however, since this paper is focused on the overall framework for indoor mobility system, the values of σ_{xx} is assumed to be fixed for all people when conducting experiments.

C. Model Predictive Control-based Planner Design

To achieve real-time computational efficiency, both the nonlinear kinematic motion equations and the PS field were approximated using the Taylor series. Specifically, the nominal points for the kinematic model were selected as the current state and control inputs measurements. For the PS field, the nominal points were defined as the predicted positions of the humans over the prediction horizon, N_p , obtained using the Constant Velocity and Turning Rate (CVTR) model. This approximation ensures the optimization problem is quadratic, allowing it to be efficiently solved using the OSQP solver [38].

The proposed MPC consists of three objective terms and a set of constraints. Equ. 18 is the cost function of the MPC; Specifically, J_1 is the PS field, which serves as a penalty as robot enters human's personal space, where, N_{human} denotes the number of humans in the environment and $PS(q)$ represents the social cost associated with the q th human; J_2 penalizes the tracking error between the predicted output η and η_{ref} throughout the prediction horizon, N_p , weighted by the positive definite matrix Q ; J_3 regulates the front and rear wheels' steering action $\delta = [\delta_f \ \delta_r]^T$ and the deviation of the robot front and rear wheels' velocity $V = [v_f \ v_r]^T$ from its reference $V_{ref} = [v_{f,ref} \ v_{r,ref}]^T$ over the control horizon N_c , with weighting matrices R and T , respectively.

Furthermore, Equ. 21 and 22 describe the motion model of the robot by using the kinematic model as in the discrete time domain, where A_k , B_k , and C_k are the linearized system matrices at time step k , and d_k represents model mismatch terms compared with the nonlinear model. Constraints are imposed on both the control increment and the absolute control input using Equ. 23 and Equ. 24, where $\Delta u_{c \min}$ and $\Delta u_{c \max}$ denote the lower and upper bounds of control rate changes, and $u_{c \min}$ and $u_{c \max}$ define the control limits. In addition, the inequality Equ. 25 is a linearized wheel-speed constraint designed to prevent slippage due to speed differences between the front and rear wheels in the body-fixed frame, where $g(u_c) = |v_f \cos(\delta_f) - v_r \cos(\delta_r)|$ is the nonlinear wheel difference expression; $E(u_c)$ is the grandiant of the function g with respect of u_c . Without this constraint, the motion planner may generate control inputs that violate the non-slip assumption in the kinematic motion model, potentially leading to unreliable or unsafe robot behaviour. Additional details regarding this constraint can be found in [8]. Finally, Equ. 26 specifies the initial condition of the optimization problem as the system states at the current time step.

$$\arg \min_{u_c} J = J_1 + J_2 + J_3 \quad (18)$$

where,

$$J_1 = \sum_{q=1}^{N_{human}} PS(q), J_2 = \sum_{i=0}^{N_p-1} \|\eta(k+i+1) - \eta_{Ref}\|_Q^2 \quad (19)$$

$$J_3 = \sum_{j=0}^{N_c-1} \|\delta(k+j)\|_R^2 + \|V(k+j) - V_{Ref}\|_T^2 \quad (20)$$

s.t.

$$\zeta(k+i+1) = A_k \zeta(k+i) + B_k u_c(k+j) + d_k(k+i) \quad (21)$$

$$\eta(k+i+1) = C_k \zeta(k+i+1) \quad (22)$$

$$\Delta u_{c \min} \leq \Delta u_c(k+j) \leq \Delta u_{c \max} \quad (23)$$

$$u_{c \min} \leq u_c(k+j) \leq u_{c \max} \quad (24)$$

$$|E(u_c(0))u_c(k+j) + g(u_c(0))| \leq 0.1 \quad (25)$$

$$\zeta(k) = \zeta(0) \quad (26)$$

VI. EXPERIMENTS

In this section, we present experimental results to evaluate the effectiveness and practicality of the proposed SAP-CoPE framework. We first validate the perception system to verify that its detection accuracy compares with baseline methods, and also in the presence of computation and communication delays. We then evaluate the overall system across a range of scenarios with different numbers of humans, with focus on the motion planning system and comparison with other planning algorithms.

TABLE II: Pose Estimation Performance Evaluation

Method	Position Error (m)	Yaw Error (deg)
	MAE / RMSE	MAE / RMSE
3DNet	0.1795 / 0.2163	8.5629 / 12.1001
Mettrabs	0.2294 / 0.2926	8.1819 / 11.2037
Cam-only	0.1098 / 0.1308	8.5199 / 11.7416
Cam+LiDAR	0.0892 / 0.1090	7.9168 / 11.0136
Cam-only (coop)	0.1087 / 0.1237	8.1727 / 10.2264
Cam+LiDAR (coop)	0.0771 / 0.0862	6.8607 / 8.9542

TABLE III: Delay mitigation evaluation results

Delay	Mode	F1	Recall	Avg. DE	Avg. AE
0ms	Baseline	0.9456	0.9512	0.0829	7.2475
	Delay-Aware	0.9485	0.9739	0.0818	5.9557
50ms	Baseline	0.9456	0.9510	0.0864	7.2314
	Delay-Aware	0.9480	0.9739	0.0840	6.1045
100ms	Baseline	0.9455	0.9510	0.0975	7.2110
	Delay-Aware	0.9480	0.9738	0.0876	6.2546
200ms	Baseline	0.9449	0.9513	0.1439	7.2365
	Delay-Aware	0.9479	0.9740	0.0993	6.5910

A. Perception Experiments

1) *Evaluation Metrics*: To rigorously evaluate the performance of the proposed 3D human pose estimation method, we use two principal metrics, compared against annotated ground truth data: Mean Absolute Error (MAE) and Root Mean Square Error (RMSE). The MAE reflects the average magnitude of estimation errors, while RMSE captures the standard deviation and sensitivity to outliers. The evaluation metrics specifically include **position error** (measured in meters) and **yaw error** (measured in degrees for orientation).

2) *Results*: We evaluate both pose estimation accuracy and system robustness under computation and communication delay. For pose estimation, we compare six configurations: learning-based baselines (3DNet [39], Mettrabs [40]), single-node camera-only and camera-LiDAR fusion, and their cooperative multi-node counterparts. Quantitative metrics are shown in Table II, and spatial error distributions are visualized in Figs. 5 and 6.

Position error: Integrating LiDAR measurements consistently improves localization accuracy over camera-only methods. Single-node camera-LiDAR fusion reduces MAE from 0.1098 m to 0.0892 m. When cooperative perception is used to refine the pose using multi-view data, performance further improves: Cam+LiDAR (coop) achieves the lowest error of 0.0771 m MAE and 0.0862 m RMSE, outperforming all baselines. The advantages of the proposed method can be further highlighted by the spatial heatmaps (Fig. 5). The learning-based methods show significant degradation in distant areas, mainly because they generalize poorly under highly varying perspective views. In contrast, the proposed methods, even the camera-only version, maintains consistently lower errors. This improvement comes from our uncertainty-aware pose estimation, which explicitly models the camera projection process and propagates measurement uncertainty through the geometry, yielding more reliable estimates in distant and low-observability regions.

Yaw error: Orientation estimation shows smaller but consistent improvements. While LiDAR provides limited direct

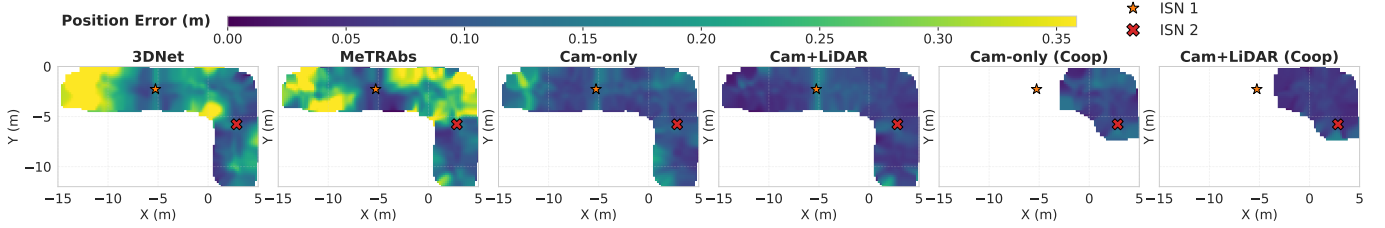


Fig. 5: Spatial distribution of position errors.

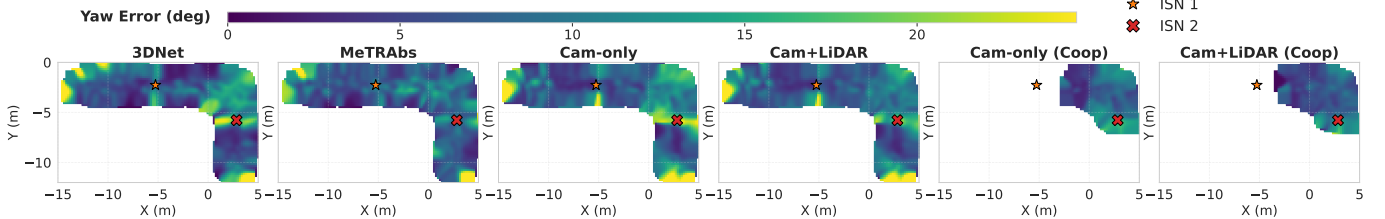


Fig. 6: Spatial distribution of yaw errors.

orientation cues, cooperative multi-view observations help stabilize heading estimation. Cam+LiDAR (coop) reduces yaw MAE to 6.86° , compared to 8.52° for camera-only and over 8° for learning-based baselines. This demonstrates that multi-view geometric consistency is particularly beneficial for resolving ambiguous orientations under occlusions.

3) *Delay Robustness Evaluation*: In our system, local perception requires an average of 42 ms, while communication latency is approximately 3 ms over local Wi-Fi and 53 ms over 5G; global fusion and tracking add a further 2 ms [6]. Consequently, practical deployments may experience total latency ranging from tens to hundreds of milliseconds. To quantify robustness to latency, we evaluate performance under simulated communication delays from 0 to 200 ms, with results summarized in Table III.

The baseline method directly fuses all received observations without multi-object tracking and delay compensation, while the proposed delay-aware pipeline incorporates timestamp-based delay correction and motion prediction. Across all delay settings, the delay-aware pipeline preserves stable perception quality and consistently outperforms the baseline, yielding higher recall as well as lower displacement error (Avg. DE) and angular error (Avg. AE). The advantage becomes more obvious as delays increase: at 200 ms, the baseline position error rises to 0.1439 m, whereas the delay-aware approach limits it to 0.0993 m. Similarly, the yaw error decreases from 7.24° to 6.59° . These results indicate that timestamp-based compensation coupled with motion prediction effectively mitigates stale observations and improves temporal consistency under significant communication latency.

4) *Discussion*: The experiments highlight:

- LiDAR fusion significantly improves positional accuracy by providing reliable depth constraints.
- Cooperative multi-node perception reduces occlusion and improves both position and heading estimation through multi-view redundancy.
- The delay-aware fusion strategy maintains high accuracy

TABLE IV: Robot and MPC Parameters. Units for velocity (or acceleration) are in [m/s] (or [m/s²]), and steering angles (or steering rate) are in [rad] (or [rad/s]).

Symbol	Value	Symbol	Value
l_f, l_r	1.2 m	$u_{c \max}$	$\left[0.7, 0.7, \frac{\pi}{2}, \frac{\pi}{2}\right]$
T_s	0.1 sec	$u_{c \min}$	$-\left[0.7, 0.7, \frac{\pi}{2}, \frac{\pi}{2}\right]$
N_p	20	$\Delta u_{c \max}$	$\left[1, 1, \frac{\pi}{24}, \frac{\pi}{24}\right]$
N_c	10	$\Delta u_{c \min}$	$-\left[1, 1, \frac{\pi}{24}, \frac{\pi}{24}\right]$

under latency, crucial for real-world deployments with computation and communication delays.

Together, these components enable accurate and robust human pose estimation suitable for real-time indoor robot navigation in crowded and communication-constrained environments.

B. Combined Experiments

As the performance of the perception of the SAP-CoPE system was already validated in the previous section, the main focus in this section is focus on the motion planning system of the proposed system by using the proposed perception system. The perception results with computation and communication delay mitigation are sent to all motion planners, including the baseline planners. The experiments were conducted in a hallway-like environment with a straight and a 90-degree turn setup. During the experiments, the robot should follow the predefined reference trajectory while proactively avoiding humans.

1) *Mobile Robot*: The robot is retrofitted based on an existing medical bed. A picture of the robot is shown in Fig. 2, in the "Application Layer" block. To ensure optimal traction and handling, the robot incorporates a two-wheel-drive system (one wheel in the front and one in the back) and an independent steering system, allowing each wheel to turn independently for omnidirectional mobility.

TABLE V: Statistics Results Comparison between the Proposed Method and Other Methods

# Human	Clearance (Avg. / Std.) [m]			Traveled Distance (Avg. / Std.) [m]			Traveled Time (Avg. / Std.) [sec.]		
	SFM	MPC + PF	Proposed	SFM	MPC + PF	Proposed	SFM	MPC + PF	Proposed
2	0.23 / 0.055	0.39 / 0.052	0.37 / 0.063	12.04 / 0.18	12.19 / 0.15	12.18 / 0.19	18.10 / 0.22	17.78 / 0.15	17.75 / 0.18
4	0.089 / 0.051	0.21 / 0.075	0.27 / 0.064	12.08 / 0.12	12.22 / 0.23	12.37 / 0.19	18.61 / 0.42	18.93 / 0.74	18.35 / 0.28
6	0.020 / 0.028	0.11 / 0.087	0.26 / 0.042	21.16 / 0.62	21.86 / 0.59	20.76 / 0.18	34.18 / 2.82	33.43 / 1.58	30.73 / 0.39

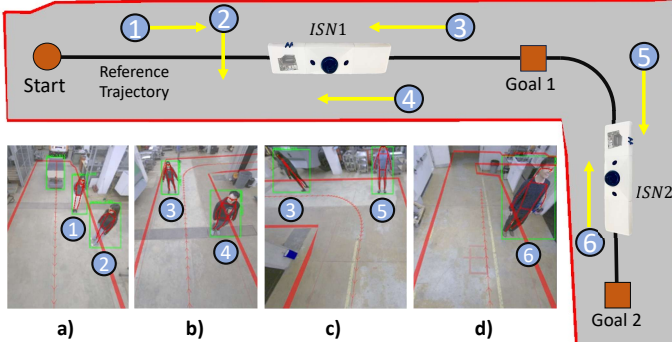


Fig. 7: Experiment setup with all participants. Images captured from a) ISN1's left camera. b) ISN1's right camera. c) ISN2's left camera. d) ISN2's right camera.

2) *Experiments Setup*: The proposed perception system and planner were implemented and tested in experiments using the C++ and Python platforms. To verify our proposed planner, we directly send the generated control inputs to the robot for simplicity. The parameters for the robot and the MPC motion planner are summarized in the table IV. All computations in the CL, including global perception fusion and motion planning algorithm are carried out on a Linux-based desktop equipped with an Intel i7-14700F CPU and 64GB of RAM.

The participant's initial position (numbered blue circles), movement direction (yellow arrow), and ISNs' location can be found in Fig. 7. Three experimental scenarios were set up to validate the proposed system. In scenario (1), which involved 2 participants, the robot was asked to follow the reference path and stop at "Goal 1", while participants 3 and 4 were involved. In scenario (2), which involved 4 participants, the goal of the robot and the movement of participants 3 and 4 remained the same, but with the addition of participants 2 and 4. In scenario (3), which involved all participants, the goal of the robot was set to "goal 2", and participants 1 to 4 remained the same, but with the addition of participants 5 and 6.

3) *Evaluation Metrics*: Three evaluation metrics were used to validate the performance of the proposed motion planning algorithm when compared with other baselines. a) **Clearance**: this metric measures the minimum distance between the robot and the human (between borders). Lower values indicate the robot is close to the human, and may increase the psychological pressure on the human and collision risk. b) **Travel Distance**: this metric measures the total travelled distance of the robot from the starting position to the goal, which reflects the travel efficiency of the robot. c) **Travel Time**: this metric measures the total travelled time of the robot from the start position to the goal, which also reflects the motion smoothness. A short travel time indicates the robot can maintain a defined speed without too much deceleration or stopping.

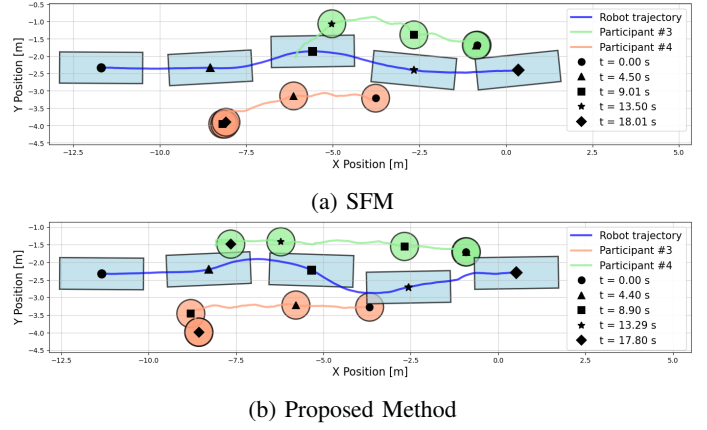


Fig. 8: 2-Participant Experiment Scenario. Trajectory plots for a) Social Force Model (SFM); b) Proposed method that combines MPC and PS model

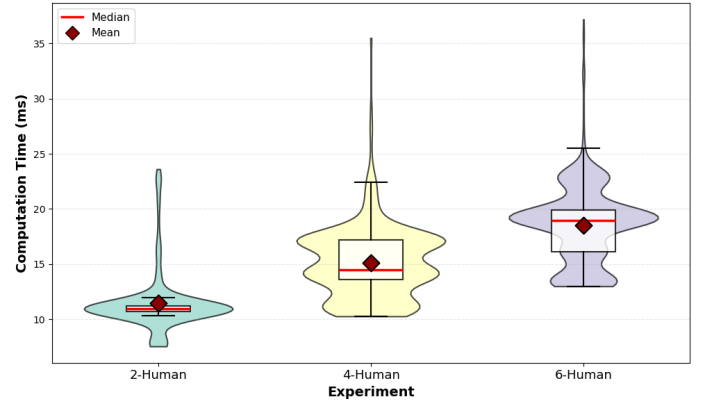


Fig. 9: Proposed Motion Planning Method Computation Time Distribution

4) *Results*: The proposed planner method, among other selected baseline methods, was tested for each scenario described in Fig. 7. The first baseline is the conventional Social Force Model (SFM) [41]. Some modifications were made to allow the algorithm to consider the shape of the robot as a rectangle. The second baseline is the MPC with the Potential Field (MPC + PF) [42]. Each method for each scenario was repeated 10 times to reduce the effect of randomness.

The results in Table V demonstrate that the proposed method achieved best overall performance than the other methods in general; specifically, the proposed method maintained an appropriate clearance to participants, a reasonable total travelled distance and the shortest travelled time through all experiments. The results also show that the clearance is decreasing for the baseline methods as the number of participants increases, but the proposed method can maintain

a proper clearance. More detailed discussion of the results can be found in the later section.

On the other hand, Fig. 9 presents an analysis of the proposed planner's computational performance across three experimental scenarios with varying numbers of dynamic obstacles. The visualization employs violin plots (mirrored distribution plot), combined with box plot elements, to comprehensively represent the distribution characteristics of computation times.

By observing the figure, one can see that the 2-Human experiment exhibits the tightest distribution (median 11 ms, mean 11.5 ms) with minimal variability, while the 4-Human scenario shows a moderate increase (median 14 ms, mean 15 ms) with occasional outliers up to 36 ms, indicating periodic solver convergence challenges. The 6-Human experiment demonstrates the highest computational burden (median 19 ms, mean 18.7 ms) with broader distribution spanning 13-26 ms and outliers approaching 37 ms, reflecting the increased optimization complexity of dense multi-obstacle configurations where additional solver iterations are occasionally required. In summary, all scenarios maintain computation times (including perception and motion planner) well below the MPC loop periods (100 ms in our case) for autonomous navigation systems, confirming real-time feasibility.

5) *Discussion:* As shown in Table V, the conventional SFM algorithm results in the smallest clearance among all compared methods. This is because the equivalent steering angles and wheel velocities of the front and rear wheels are computed based on the optimal CG. velocity and heading angle obtained from the algorithm; consequently, the robot's omnidirectional maneuverability is not explicitly considered. As illustrated in Fig. 8, due to the robot's length, participants may need to actively dodge the robot when the SFM is applied. In contrast, when omnidirectional motion capability is incorporated, the robot can smoothly avoid all participants without causing any disturbances.

Furthermore, it is worth noting that the MPC+PF method exhibits relatively long travel times in the 4-human and 6-human scenarios. This is because the potential field employed in this approach is more conservative than that of the PS field; consequently, the robot occasionally needs to reduce its speed when navigating through crowds. This behaviour is also reflected in the reduction of the clearance metric, particularly in the 6-participant scenarios. Although this characteristic allows the robot to maintain larger distances from participants in relatively sparse environments, it may pose safety concerns in densely populated settings, as unexpected deceleration could cause participants to collide with the robot, especially for those approaching the robot from behind.

In summary, the SFM has relatively worse performance because it does not account for the robot's omnidirectional maneuverability. The MPC+PF method performs comparably to the proposed approach in less crowded scenarios and can even maintain larger clearances; however, due to its symmetric field representation, its performance decreases significantly in more challenging and densely populated environments.

VII. CONCLUSIONS AND FUTURE WORK

In this paper, we propose a SAP-CoPE framework for autonomous driving systems operating in human-populated environments. By leveraging a cooperative infrastructure sensor network and a novel 3D human pose estimation method, our approach effectively addresses perception limitations and occlusion challenges of accurate human intention recognition and safe navigation. Additionally, the integration of human-pose-based PS field into an MPC controller enables the generation of trajectories that prioritize human comfort. Extensive evaluations in real-world environments validate the effectiveness of our proposed SAP-CoPE framework. Due to the modular design and real-time performance, our proposed SAP-CoPE framework has strong potential for deployment in practical applications such as indoor service robots, healthcare logistics, and autonomous navigation in shared public spaces. Future work will focus on enhancing system robustness in highly dynamic environments and further improving human intention prediction with the combination of learning-based algorithms.

ACKNOWLEDGMENT

The authors gratefully acknowledge the financial support of the Natural Sciences and Engineering Research Council of Canada (NSERC) and MITACS, as well as the financial and technical support provided by Rogers Communications Inc. Canada.

REFERENCES

- [1] M. Law, H. S. Ahn, E. Broadbent, K. Peri, N. Kerse, E. Topou, N. Gasteiger, and B. MacDonald, "Case studies on the usability, acceptability and functionality of autonomous mobile delivery robots in real-world healthcare settings," *Intelligent Service Robotics*, vol. 14, no. 3, pp. 387–398, 2021.
- [2] H. Pikner, R. Sell, K. Karjust, E. Malayjerdi, and T. Velsker, "Cyber-physical control system for autonomous logistic robot," in *2021 IEEE 19th International Power Electronics and Motion Control Conference (PEMC)*. IEEE, 2021, pp. 699–704.
- [3] I. H. Savci, A. Yilmaz, S. Karaman, H. Ocakli, and H. Temeltas, "Improving navigation stack of a ros-enabled industrial autonomous mobile robot (amr) to be incorporated in a large-scale automotive production," *The International Journal of Advanced Manufacturing Technology*, vol. 120, no. 5, pp. 3647–3668, 2022.
- [4] D. K. Kim and S. Park, "An analysis of the effects of occupational accidents on corporate management performance," *Safety science*, vol. 138, p. 105228, 2021.
- [5] L. Schmid, O. Andersson, A. Sulser, P. Pfreundschuh, and R. Siegwart, "Dynablox: Real-time detection of diverse dynamic objects in complex environments," *IEEE Robotics and Automation Letters*, vol. 8, no. 10, pp. 6259–6266, 2023.
- [6] M. Ning, Y. Cui, Y. Yang, S. Huang, Z. Liu, A. R. Alghooneh, E. Hashemi, and A. Khajepour, "Enhancing indoor mobility with connected sensor nodes: A real-time, delay-aware cooperative perception approach," in *2024 IEEE 27th International Conference on Intelligent Transportation Systems (ITSC)*, 2024, pp. 1139–1144.
- [7] C. Sun, R. Zhang, A. R. Alghooneh, M. Ning, P. Panahandeh, S. Tuer, and A. Khajepour, "Cascaded safety analysis and test scenario generation techniques for autonomous driving: A case study with watonobus," *Automotive Innovation*, pp. 1–12, 2025.
- [8] Y. Yang, M. Ning, S. Huang, E. Hashemi, and A. Khajepour, "Intelligent mobility system with integrated motion planning and control utilizing infrastructure sensor nodes," in *2024 IEEE 27th International Conference on Intelligent Transportation Systems (ITSC)*, 2024, pp. 1133–1138.
- [9] S. Nonaka, K. Inoue, T. Arai, and Y. Mae, "Evaluation of human sense of security for coexisting robots using virtual reality. 1st report: evaluation of pick and place motion of humanoid robots," in *IEEE International Conference on Robotics and Automation, 2004. Proceedings. ICRA'04. 2004*, vol. 3. IEEE, 2004, pp. 2770–2775.

- [10] B. Zhou, X. Wang, and X. Tang, "Understanding collective crowd behaviors: Learning a mixture model of dynamic pedestrian-agents," in *2012 IEEE Conference on Computer Vision and Pattern Recognition*. IEEE, 2012, pp. 2871–2878.
- [11] T. A. Heya, S. E. Arefin, A. Chakrabarty, and M. Alam, "Image processing based indoor localization system for assisting visually impaired people," in *2018 Ubiquitous Positioning, Indoor Navigation and Location-Based Services (UPINLBS)*. IEEE, 2018, pp. 1–7.
- [12] A. Haque, M. Guo, A. Alahi, S. Yeung, Z. Luo, A. Rege, J. Jopling, L. Downing, W. Beninati, A. Singh, T. Platchek, A. Milstein, and L. Fei-Fei, "Towards vision-based smart hospitals: A system for tracking and monitoring hand hygiene compliance," in *Proceedings of the 2nd Machine Learning for Healthcare Conference*, ser. Proceedings of Machine Learning Research, F. Doshi-Velez, J. Fackler, D. Kale, R. Ranganath, B. Wallace, and J. Wiens, Eds., vol. 68. PMLR, 18–19 Aug 2017, pp. 75–87. [Online]. Available: <https://proceedings.mlr.press/v68/haque17a.html>
- [13] Á. Carro-Lagoa, V. Barral, M. González-López, C. J. Escudero, and L. Castedo, "Multicamera edge-computing system for persons indoor location and tracking," *Internet of Things*, vol. 24, p. 100940, 2023.
- [14] D. Bršćić, T. Kanda, T. Ikeda, and T. Miyashita, "Person tracking in large public spaces using 3-d range sensors," *IEEE Transactions on Human-Machine Systems*, vol. 43, no. 6, pp. 522–534, 2013.
- [15] A. Rudenko, T. P. Kucner, C. S. Swaminathan, R. T. Chadalavada, K. O. Arras, and A. J. Lilienthal, "Thör: Human-robot navigation data collection and accurate motion trajectories dataset," *IEEE Robotics and Automation Letters*, vol. 5, no. 2, pp. 676–682, 2020.
- [16] S. Adnan Yusuf, A. Khan, and R. Souissi, "Vehicle-to-everything (v2x) in the autonomous vehicles domain – a technical review of communication, sensor, and ai technologies for road user safety," *Transportation Research Interdisciplinary Perspectives*, vol. 23, p. 100980, 2024.
- [17] T. Huang, J. Liu, X. Zhou, D. C. Nguyen, M. R. Azghadi, Y. Xia, Q.-L. Han, and S. Sun, "V2x cooperative perception for autonomous driving: Recent advances and challenges," *arXiv preprint arXiv:2310.03525*, 2023.
- [18] Z. Bai, G. Wu, M. J. Barth, Y. Liu, E. A. Sisbot, K. Oguchi, and Z. Huang, "A survey and framework of cooperative perception: From heterogeneous singleton to hierarchical cooperation," *IEEE Transactions on Intelligent Transportation Systems*, 2024.
- [19] A. Caillot, S. Ouerghi, P. Vasseur, R. Boutteau, and Y. Dupuis, "Survey on cooperative perception in an automotive context," *IEEE Transactions on Intelligent Transportation Systems*, vol. 23, no. 9, pp. 14 204–14 223, 2022.
- [20] J. Wang, S. Tan, X. Zhen, S. Xu, F. Zheng, Z. He, and L. Shao, "Deep 3d human pose estimation: A review," *Computer Vision and Image Understanding*, vol. 210, p. 103225, 2021.
- [21] A. Zanfir, M. Zanfir, A. Gorban, J. Ji, Y. Zhou, D. Anguelov, and C. Sminchisescu, "Hum3dil: Semi-supervised multi-modal 3d human-pose estimation for autonomous driving," in *Conference on Robot Learning*. PMLR, 2023, pp. 1114–1124.
- [22] P. Bauer, A. Bouazizi, U. Kressel, and F. B. Flohr, "Weakly supervised multi-modal 3d human body pose estimation for autonomous driving," in *2023 IEEE Intelligent Vehicles Symposium (IV)*. IEEE, 2023, pp. 1–7.
- [23] J. Chen, X. Chen, and S. Liu, "Trajectory planning of autonomous mobile robot using model predictive control in human-robot shared workspace," in *2023 IEEE 3rd International Conference on Electronic Technology, Communication and Information (ICETCI)*. IEEE, 2023, pp. 462–467.
- [24] F. Fang, X. Wang, Z. Li, K. Qian, and B. Zhou, "A unified framework for pedestrian trajectory prediction and social-friendly navigation," *IEEE Transactions on Industrial Electronics*, 2023.
- [25] K. Shu, R. V. Mehrizi, S. Li, M. Pirani, and A. Khajepour, "Human inspired autonomous intersection handling using game theory," *IEEE Transactions on Intelligent Transportation Systems*, vol. 24, no. 10, pp. 11 360–11 371, 2023.
- [26] K. Shu, A. R. Alghooneh, M. Ning, S. Li, M. Pirani, and A. Khajepour, "Game-theory in practice: Application to motion planning and decision making in an autonomous shuttle bus," *IEEE Transactions on Intelligent Transportation Systems*, 2024.
- [27] M. Kamezaki, Y. Tsuburaya, T. Kanada, M. Hirayama, and S. Sugano, "Reactive, proactive, and inducible proximal crowd robot navigation method based on inducible social force model," *IEEE Robotics and Automation Letters*, vol. 7, no. 2, pp. 3922–3929, 2022.
- [28] P. Ratsamee, Y. Mae, K. Ohara, T. Takubo, and T. Arai, "Human-robot collision avoidance using a modified social force model with body pose and face orientation," *International Journal of Humanoid Robotics*, vol. 10, no. 01, p. 1350008, 2013.
- [29] X.-T. Truong and T. D. Ngo, "Toward socially aware robot navigation in dynamic and crowded environments: A proactive social motion model," *IEEE Transactions on Automation Science and Engineering*, vol. 14, no. 4, pp. 1743–1760, 2017.
- [30] I. S. Mohamed, M. Ali, and L. Liu, "Chance-constrained sampling-based mpc for collision avoidance in uncertain dynamic environments," *IEEE Robotics and Automation Letters*, 2025.
- [31] T. D. Ngo, X.-T. Truong *et al.*, "Socially aware robot navigation framework: Where and how to approach people in dynamic social environments," *IEEE Transactions on Automation Science and Engineering*, vol. 20, no. 2, pp. 1322–1336, 2022.
- [32] R. Khanam and M. Hussain, "Yolov11: An overview of the key architectural enhancements," 2024. [Online]. Available: <https://arxiv.org/abs/2410.17725>
- [33] T.-Y. Lin, M. Maire, S. Belongie, L. Bourdev, R. Girshick, J. Hays, P. Perona, D. Ramanan, C. L. Zitnick, and P. Dollár, "Microsoft coco: Common objects in context," 2015.
- [34] T. Amaoka, H. Laga, S. Saito, and M. Nakajima, "Personal space modeling for human-computer interaction," in *Entertainment Computing–ICEC 2009: 8th International Conference, Paris, France, September 3-5, 2009. Proceedings 8*. Springer, 2009, pp. 60–72.
- [35] E. T. Hall, R. L. Birdwhistell, B. Bock, P. Bohannon, A. R. Diebold Jr, M. Durbin, M. S. Edmonson, J. Fischer, D. Hymes, S. T. Kimball *et al.*, "Proxemics [and comments and replies]," *Current anthropology*, vol. 9, no. 2/3, pp. 83–108, 1968.
- [36] R. Sommer, "Personal space. the behavioral basis of design." 1969.
- [37] S. Shozo, "Comfortable distance between people: Personal space," 1990.
- [38] B. Stellato, G. Banjac, P. Goulart, A. Bemporad, and S. Boyd, "OSQP: an operator splitting solver for quadratic programs," *Mathematical Programming Computation*, vol. 12, no. 4, pp. 637–672, 2020.
- [39] J. Martinez, R. Hossain, J. Romero, and J. J. Little, "A simple yet effective baseline for 3d human pose estimation," in *Proceedings of the IEEE international conference on computer vision*, 2017, pp. 2640–2649.
- [40] I. Sárándi, A. Hermans, and B. Leibe, "Learning 3d human pose estimation from dozens of datasets using a geometry-aware autoencoder to bridge between skeleton formats," in *Proceedings of the IEEE/CVF Winter Conference on Applications of Computer Vision*, 2023, pp. 2956–2966.
- [41] D. Helbing and P. Molnar, "Social force model for pedestrian dynamics," *Physical review E*, vol. 51, no. 5, p. 4282, 1995.
- [42] Y. Rasekhipour, A. Khajepour, S.-K. Chen, and B. Litkouhi, "A potential field-based model predictive path-planning controller for autonomous road vehicles," *IEEE Transactions on Intelligent Transportation Systems*, vol. 18, no. 5, pp. 1255–1267, 2016.



Minghao Ning received the B.S. degree in Vehicle Engineering from the Beijing Institute of Technology, Beijing, China, in 2020. He is currently pursuing a Ph.D. degree with the Department of Mechanical and Mechatronics Engineering, University of Waterloo. His research interests include autonomous driving, LiDAR perception, planning and control.



Yufeng Yang is a Ph.D. candidate at the University of Waterloo Mechatronic Vehicle Systems (MVS) Lab. He received his B.Sc. degree in Mechanical Engineering with a minor in Mechatronics from the University of Calgary in 2021. His primary research interests include omnidirectional mobile robots, motion planning, control, and human-robot interaction.



Shucheng Huang is currently a Ph.D. candidate at the University of Waterloo Mechatronic Vehicle Systems (MVS) Lab and ComplING Lab and a graduate student member at the Vector Institute. He received the MASc degree in mechanical and mechatronics engineering from the University of Waterloo in 2020 and the B.S. degree in mechanical engineering from Penn State University in 2018. His research interests include applications of LLM in autonomous driving, learning-based planning, and natural language processing.



Amir Khajepour is a professor of Mechanical and Mechatronics Engineering and the Director of the Mechatronic Vehicle Systems (MVS) Lab at the University of Waterloo. He held the Tier 1 Canada Research Chair in Mechatronic Vehicle Systems from 2008 to 2022 and the Senior NSERC/General Motors Industrial Research Chair in Holistic Vehicle Control from 2017 to 2022. His work has led to the training of over 150 PhD and MASc students, filing over 30 patents, publication of 600 research papers, numerous technology transfers, and the establishment of several start-up companies. He has been recognized with the Engineering Medal from Professional Engineering Ontario and is a fellow of the Engineering Institute of Canada, the American Society of Mechanical Engineering, and the Canadian Society of Mechanical Engineering.



Jiaming Zhong is currently a Ph.D. candidate at the University of Waterloo Mechatronic Vehicle Systems (MVS) Lab. He received the B.S. and the MASc degrees in mechanical engineering from Beijing Institute of Technology, China, in 2014 and 2017. His research interests include learning-based planning and control, multi-agent theory, and autonomous driving.



Keqi Shu is a postdoctoral research fellow in Mechanical and Mechatronics Engineering at the University of Waterloo. His research interests involve interactive planning and decision-making of autonomous vehicles. He completed his PhD and Master's degree in Mechanical and Mechatronics Engineering in the University of Waterloo, Ontario, Canada, and his B.Sc. degree in Northwestern Polytechnical University, Xi'an Shaanxi, China.



Chen Sun received the Ph.D. degree in Mechanical & Mechatronics Engineering from University of Waterloo, ON, Canada in 2022, M.A.Sc degree in Electrical & Computer Engineering from University of Toronto, ON, Canada in 2017 and B.Eng. degree in automation from the University of Electronic Science and Technology of China, Chengdu, China, in 2014. He is currently an Assistant Professor with the Department of Data and Systems Engineering, University of Hong Kong. His research interests include field robotics, safe and trustworthy autonomous driving and in general human-CPS autonomy.



Ehsan Hashemi received his Ph.D. in Mechanical and Mechatronics Engineering in 2017 from the University of Waterloo, ON, Canada; M.Sc. in Mechanical Engineering in 2005 from Amirkabir University of Technology (Tehran Polytechnic). He is currently an Assistant Professor at the Department of Mechanical Engineering, University of Alberta. His research interests are robotics, control theory, distributed estimation, and human-robot interaction.